Optomechanical Transducers for Long-Distance Quantum Communication

K. Stannigel,[1] P. Rabl,[2,1] A. S. Sørensen,[3] P. Zoller,[1] and M. D. Lukin[2,4]

[1]*Institute for Quantum Optics and Quantum Information, 6020 Innsbruck, Austria, and Institute for Theoretical Physics, University of Innsbruck, 6020 Innsbruck, Austria*

[2]*Institute for Theoretical Atomic, Molecular and Optical Physics, Cambridge, Massachusetts 02138, USA*

[3]*QUANTOP, Niels Bohr Institute, University of Copenhagen, DK-2100 Copenhagen Ø, Denmark*

[4]*Physics Department, Harvard University, Cambridge, Massachusetts 02138, USA*

(Received 23 June 2010; published 23 November 2010)

We describe a new scheme to interconvert stationary and photonic qubits which is based on indirect qubit-light interactions mediated by a mechanical resonator. This approach does not rely on the specific optical response of the qubit and thereby enables optical quantum interfaces for a wide range of solid state spin and charge based systems. We discuss the implementation of state transfer protocols between distant nodes of a quantum network and show that high transfer fidelities can be achieved under realistic experimental conditions.

DOI: 10.1103/PhysRevLett.105.220501 PACS numbers: 03.67.Hk, 07.10.Cm, 42.50.Wk

Many quantum information applications rely on efficient ways to distribute quantum states either within a large computing architecture or over long distances for quantum communication. For this purpose optical "flying" qubits play a unique role and the ability to interconvert "stationary" qubits and photons is a key element in quantum computing and quantum communication architectures. Light-matter interfaces and state transfer protocols have been proposed and first implemented with atomic systems using cavity QED [1,2]. In light of the remarkable progress in nanoengineered solid state quantum systems, the challenge is now to develop equivalent optical interfaces for a broad range of solid state spin [3] and charge [4,5] based qubits. A promising avenue towards this goal is provided by optonanomechanics [6–8], where a nanoscale mechanical oscillator can be coherently coupled to light. As described below, this provides a natural setting for an optomechanical transducer (OMT), where indirect qubit-photon interactions are mediated by vibrations of a macroscopic mechanical device.

The setup of Fig. 1 describes a quantum network where the nodes are represented by solid state qubits and the quantum channel by an optical fiber. The qubits are encoded in electronic spin or charge degrees of freedom and coupled to the motion of a mechanical beam via magnetic [9,10] or electrostatic forces [11,12]. At the same time the resonator interacts with the evanescent field of a toroidal microcavity as recently demonstrated by Anetsberger *et al.* [6]. Excitations from the qubit can be transferred to the mechanical oscillator and then mapped onto a traveling photon in a process which does not rely on optical properties of the qubit and allows the qubit to be spatially separated from the light field. Therefore, this scheme is suited for various solid state spin, charge, or superconducting qubits which do not interact coherently with light and provides a basic building block for many optical quantum communication applications.

A fundamental task in optical quantum networks is the implementation of a state transfer protocol $(\alpha|0\rangle_i + \beta|1\rangle_i)|0\rangle_j \rightarrow |0\rangle_i(\alpha|0\rangle_j + \beta|1\rangle_j)$ between two remote qubits i and j. This is achieved by converting the qubit state $|1\rangle_i$ into a photon via the OMT which then propagates along the fiber and is reabsorbed at the second node. As first outlined in atomic cavity QED [1], the theory of cascaded quantum systems [13] provides a natural framework to describe these processes and in the case of atomic qubits can be used to identify a set of laser control pulses which achieve a state transfer with unit fidelity. Here we show that OMTs allow us to generalize these ideas for a much broader range of qubits.

Model.—We model the setup shown in Fig. 1(a) by a Hamiltonian $H = \sum_{i=1}^{N} H^i_{\rm node} + H_{\rm fib}$, where $H^i_{\rm node}$ describes the dynamics of node i and $H_{\rm fib}$ accounts for the coupling between the cavities and the fiber. Following previous work [8,9,11] we obtain for each node ($\hbar = 1$)

$$H^i_{\rm node} = H^i_q + \frac{\lambda}{2}(\sigma^i_- b^\dagger_i + \sigma^i_+ b_i) + \omega_r b^\dagger_i b_i + \Delta^i_c c^\dagger_i c_i + (G_i c^\dagger_i + G^*_i c_i)(b_i + b^\dagger_i), \quad (1)$$

where σ^i_μ are Pauli operators for the qubit i, and b_i and c_i the bosonic operators for the resonator and the cavity

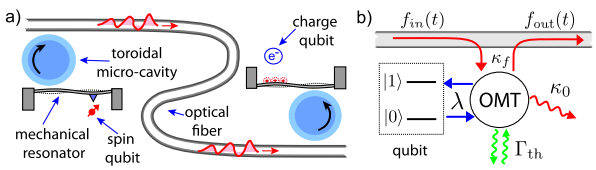

FIG. 1 (color online). (a) A quantum network where spin or charge based qubits and photons are coupled by an optomechanical transducer (OMT). (b) At each node the OMT mediates coherent coupling between the qubit and photons in the fiber, but also adds noise and loss channels in form of mechanical dissipation ($\Gamma_{\rm th}$) and intrinsic cavity decay (κ_0). See text for details.

modes, respectively. In Eq. (1) $H_q^i = \omega_q^i \sigma_z^i/2$ where ω_q^i is the tunable qubit splitting, ω_r is the mechanical vibration frequency and λ characterizes the strength of the qubit-resonator coupling which can be of magnetic [9] or electrostatic origin [11]. The last term in Eq. (1) describes the linearized optomechanical (OM) interactions for a driven cavity mode [8]. Here, $G_i = \alpha_i g_0$ is the enhanced OM coupling for a mean cavity field amplitude α_i and $g_0 = a_0(\partial\omega_c/\partial x)$ is the shift of the cavity frequency ω_c associated with the mechanical zero point oscillation a_0. For each node the coupling G_i and the detuning $\Delta_c^i = \omega_c - \omega_L - 2|G_i|^2/\omega_r$ can be controlled by the strength and the frequency ω_L of local driving fields. Note that the parallel beam orientation as in Fig. 1 causes negligible scattering between right and left circulating modes [6] which allows us to consider a single cavity mode only.

We assume that the laser-driven cavity modes couple dominantly to the right propagating field in the fiber, $f_R(t,z) = \frac{1}{\sqrt{2\pi}} \int_0^\infty f_\omega e^{-i\omega(t-z/c)} d\omega$, where $[f_\omega, f_{\omega'}^\dagger] = \delta(\omega - \omega')$. Then, $H_{\rm fib} = i\sqrt{2\kappa_f}\sum_i (c_i^\dagger f_R(t,z_i) - \text{H.c.})$, where $2\kappa_f$ is the decay rate into the fiber and $z_i < z_{i+1}$ are the cavity positions along the fiber. For each node we define in- and outfields $f_{{\rm in},i}(t) = f_R(t, z_i + 0^-)$ and $f_{{\rm out},i}(t) = f_R(t, z_i + 0^+)$ and model the resulting dissipative dynamics by quantum Langevin equations

$$\dot{c}_i = i[H_{\rm node}^i, c_i] - \kappa c_i - \sqrt{2\kappa_f} f_{{\rm in},i}(t) - \sqrt{2\kappa_0} f_{0,i}(t), \quad (2)$$

together with the relation $f_{{\rm out},i}(t) = f_{{\rm in},i}(t) + \sqrt{2\kappa_f} c_i(t)$. For the first cavity, $f_{{\rm in},1}(t)$ is a δ-correlated noise operator acting on the vacuum state while the input for the successive cavities is determined by the relation $f_{{\rm in},i}(t) = f_{{\rm out},i-1}(t - (z_i - z_{i-1})/c)$. In Eq. (2) we have introduced a total decay rate $\kappa = \kappa_0 + \kappa_f$ and the vacuum noise operators $f_{0,i}(t)$ to account for an intrinsic cavity loss rate κ_0. We must also include damping of the resonator modes which for a mechanical quality factor $Q_m = \omega_r/\gamma_m$ is described by the Langevin equations

$$\dot{b}_i = i[H_{\rm node}^i, b_i] - \frac{\gamma_m}{2} b_i - \sqrt{\gamma_m}\xi_i(t). \quad (3)$$

Here, $\langle \xi_i^\dagger(t)\xi_j(t')\rangle = N_{\rm th}\delta_{ij}\delta(t-t')$ and for temperatures $T > \hbar\omega_r/k_B$ we identify below $\Gamma_{\rm th} = \gamma_m N_{\rm th} \approx k_B T/\hbar Q_m$ as the relevant mechanical decoherence rate.

Equations (1)–(3) describe a cascaded quantum network [13] where at each node the OM system acts as a *linear* transducer between the fiber in- and outfields, the qubit state as well as thermal noise [see Fig. 1(b)]. In the absence of the qubits mechanical excitations of the OMT are converted into photons in the fiber with a rate $\gamma_{\rm op} \approx \min\{|G_i|^2\kappa/(\kappa^2 + (\Delta_c^i - \omega_r)^2), \kappa/2\}$. This rate is given by the smallest real part of the eigenvalues of the linear system (2) and (3) for $\lambda \to 0$ and is equivalent to the OM cooling rate in the weak and strong coupling regime [14]. To proceed, we focus on the experimentally relevant regime $\lambda \ll \gamma_{\rm op}$, where we can adiabatically eliminate the fast dynamics of the coupled OM degrees of freedom. As a result we obtain a master equation for the reduced qubit density operator ρ [15], which we display here for the relevant case of two qubits:

$$\dot{\rho} \simeq -i(H_{\rm eff}\rho - \rho H_{\rm eff}^\dagger) + \mathcal{S}\rho\mathcal{S}^\dagger + \mathcal{L}_{\rm noise}(\rho). \quad (4)$$

Here, $H_{\rm eff} = \sum_i H_q^i - \frac{i}{2} J_{12}(\sigma_-^1\sigma_+^2 - \sigma_+^1\sigma_-^2) - \frac{i}{2}\mathcal{S}^\dagger\mathcal{S}$ is an effective (non-Hermitian) Hamiltonian and the collective jump operator $\mathcal{S} = \sum_i \sqrt{\eta\Gamma_i}\,\sigma_-^i$ accounts for dissipation due to photons lost through the fiber. Further, $\eta = \kappa_f/\kappa$ and the decay rates $\Gamma_i = 2\,\text{Re}\{S_{ii}(\omega_q)\}$ as well as the photon mediated qubit-qubit coupling $J_{12} = |S_{21}(\omega_q)| \simeq \eta\sqrt{\Gamma_1\Gamma_2}$ are given by the spectrum $S_{ij}(\omega) = \frac{\lambda^2}{4}\int_0^\infty d\tau \langle [b_i(\tau), b_j^\dagger(0)]\rangle_0 e^{i\omega\tau}$, where the resonator equilibrium correlation functions $\langle b_i(\tau) b_i^\dagger(0)\rangle_0$ follow from the linear Langevin equations (2) and (3) in the limit $\lambda \to 0$. The last term in Eq. (4) summarizes all decoherence processes in the system and can be written as $\mathcal{L}_{\rm noise}(\rho) \simeq \frac{1}{2}\sum_i \Gamma_i N_i([\sigma_-^i, [\rho, \sigma_+^i]] + \text{H.c.}) + \mathcal{L}_{\kappa_0}(\rho)$. Here, $\mathcal{L}_{\kappa_0}(\rho) = (1-\eta)\sum_i \frac{\Gamma_i}{2}(2\sigma_-^i\rho\sigma_+^i - \{\sigma_+^i\sigma_-^i, \rho\})$ accounts for photon losses while other noise sources discussed below are described by effective thermal occupation numbers $N_i = (\lambda^2/2\Gamma_i)\text{Re}\int_0^\infty d\tau \langle b_i^\dagger(\tau) b_i(0)\rangle_0 e^{-i\omega_q\tau}$. Since coherent processes occur on a time scale Γ_i^{-1} the parameters N_i and $(1-\eta)$ quantify the imperfections of the system. Note that in Eq. (4) we have absorbed a small shift of the qubit frequencies into the ω_q^i, and phases θ_i into the qubit operators, $e^{i\theta_i}\sigma_-^i \to \sigma_-^i$, to obtain real J_{12}.

Discussion.—The first two terms in Eq. (4) represent the dynamics of an ideal cascaded qubit network [1,13]. The coherent and incoherent dynamics of the system is fully determined by the effective decay rates Γ_i, which for $\gamma_m \ll \gamma_{\rm op}$ can be approximated by

$$\Gamma_i \simeq \frac{\lambda^2|G_i|^2\kappa/2}{(|G_i|^2 + (\Delta_c^i - \omega_q^i)(\omega_q^i - \omega_r))^2 + \kappa^2(\omega_q^i - \omega_r)^2}. \quad (5)$$

For $\Delta_c^i \approx \omega_r$ exact values for Γ_i are plotted in Fig. 2(a) as a function of $|G_i|$ and ω_q. Its behavior reflects the excitation spectrum of the coupled OM modes at the qubit frequency ω_q. For $|G_i| < \kappa/2$ we have a single resonance at $\omega_q = \omega_r$ of width $\gamma_{\rm op} \simeq |G_i|^2/\kappa$. For larger $|G_i|$ a mode splitting occurs and two resonances of width $\gamma_{\rm op} \simeq \kappa/2$ appear at $\omega_\pm \simeq \sqrt{\omega_r^2 \pm 2|G_i|\omega_r}$ [14].

By adiabatically adjusting different OM parameters the qubit decay rate can be tuned within a wide range $\Gamma_{\rm res} \lesssim \Gamma_i(t) \lesssim \lambda^2/(2\gamma_{\rm op}) < \kappa$, with a small residual decay $\Gamma_{\rm res} \ll \gamma_m$ due to mechanical damping [15]. Hence, this setup is analogous to the cavity QED setting of Ref. [1] and similar arguments can be used to determine optimal control pulses for state transfer protocols. We illustrate this for two nodes where we demand that under ideal conditions $\mathcal{L}_{\rm noise} \equiv 0$,

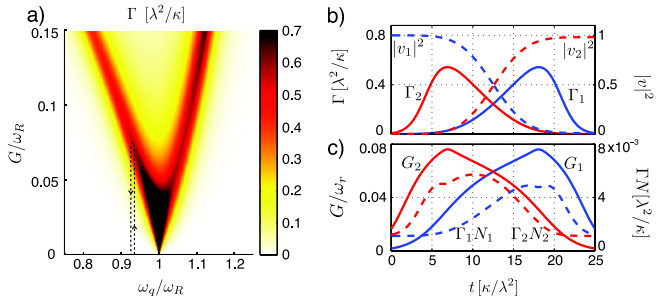

FIG. 2 (color online). (a) Effective single-qubit decay Γ as a function of G and ω_q for the parameters $\kappa_f = 0.05\omega_R$, $\kappa_0 = \gamma_m = 0$, with cavity and resonator being in resonance ($\Delta_c = \omega_R$) at $G = 1.5\kappa_f$. The dotted line indicates the control pulse shown in (c). (b) Pulse shapes for $\Gamma_{1,2}(t)$ which implement a perfect state transfer $v_2(t_f) \simeq 1$ as described in the text. (c) Control pulses for $G_{1,2}(t)$ which generate the $\Gamma_{1,2}(t)$ shown in (b). The dashed lines indicate the corresponding noise terms which appear in $\mathcal{L}_{\text{noise}}$. The parameters used for this plot are $\omega_q^{1,2} = \omega_R - 1.5\kappa_f$, $\Gamma_{th}/\kappa_f = 0.01$ and all others as in (a).

$\eta = 1$ the system remains in a pure two-qubit state $|\psi(t)\rangle = \alpha|00\rangle + \beta(v_1(t)|10\rangle + v_2(t)|01\rangle)$ for all times. This is guaranteed by imposing the dark-state condition $\mathcal{S}(t)|\psi(t)\rangle = (\sqrt{\Gamma_1(t)}\sigma_-^1 + \sqrt{\Gamma_2(t)}\sigma_-^2)|\psi(t)\rangle = 0$ which together with the evolution of $|\psi(t)\rangle$ under H_{eff} determines a set of optimal pulse shapes $\Gamma_{1,2}(t)$ [1]. A specific example of time-symmetric pulses $\Gamma_2(t) = \Gamma_1(-t)$ is shown in Fig. 2(b), where $\Gamma_1(\tilde{t} = t - t_f/2) = \Gamma_0 \exp(-c\tilde{t}^2)/(1 - \Gamma_0\sqrt{\pi/4c}\,\text{Erf}(\sqrt{c}\tilde{t}))$. Here, $\Gamma_0 = \Gamma_1(t = t_f/2)$ and $c > \pi\Gamma_0^2/4$ are used to adjust the pulse such that $|v_1(t_f)|^2 < 10^{-2}$ at the final time t_f. Figure 2(c) finally shows the corresponding control pulses $G_{1,2}(t)$ obtained via Eq. (5) which can be used to actually implement the transfer protocol by adjusting the driving strength for each cavity. Alternatively, we can identify a similar control pulse for $\Delta_c^{1,2}(t)$ and vary the cavity frequencies $\omega_c^i(t)$ [16]. In both cases the mutual dependence of G_i and Δ_c^i must be taken into account and tuning the qubit frequencies ensures that $\delta(t) \equiv \omega_q^2(t) - \omega_q^1(t) + \dot{\theta}_1(t) - \dot{\theta}_2(t) = 0$, $\forall t$.

Noise.—Under realistic conditions the OMT adds noise to the system which is characterized by $N_i \approx N_{0,i} + N_{\text{casc},i}$. Here, $N_{\text{casc},i}$ is defined below and $N_{0,i}$ accounts for noise which is generated locally by each OM system,

$$N_{0,i} \approx \frac{\Gamma_{\text{th}}}{2\kappa}\frac{\kappa^2 + (\Delta_c^i - \omega_q^i)^2}{|G_i|^2} + \frac{\kappa^2 + (\Delta_c^i - \omega_q^i)^2}{4\Delta_c^i\omega_q^i}. \quad (6)$$

The contribution $\sim\Gamma_{\text{th}}$ arises from thermal excitations of the mechanical mode while the second term results from Stokes scattering events due to energy nonconserving terms as $G_i b_i^\dagger c_i^\dagger$ in H_{node}^i. On resonance, i.e., $\Delta_c^i = \omega_r$ and $\omega_q \simeq \omega_-$, Eq. (6) is similar (but not identical) to the final occupation number in OM cooling experiments [17,18]. Therefore, the requirements for ground state cooling, namely $\Gamma_{\text{th}}/\gamma_{\text{op}} \ll 1$ and sideband resolved conditions G, $\kappa \ll \omega_r$, are, in addition to $1 - \eta \ll 1$, also sufficient to realize a low noise OMT with $N_0 \ll 1$. For multiple nodes, noise photons generated at one node can propagate along the fiber and affect successive nodes, which is described by $N_{\text{casc},i}$. For two nodes this leads to a small asymmetry between $N_1(t)$ and $N_2(t)$ as shown in Fig. 2(c), but in a larger network the scaling $N_{\text{casc},i} \sim (i - 1)N_0$ can limit the number of *active* nodes. This problem can be avoided by activating individual nodes selectively and one possible scheme to achieve this is outlined below.

To study the quantum state transfer $|\psi_0\rangle_1|0\rangle_2 \rightarrow |0\rangle_1|\psi_0\rangle_2$ under realistic conditions we numerically simulate the full master equation (4) for the control pulses described in Fig. 2. The resulting state transfer fidelity $\mathcal{F} = \langle\psi_0|\text{Tr}_1\{\rho(t_f)\}|\psi_0\rangle$ averaged over all input states $|\psi_0\rangle$ is plotted in Fig. 3(a) for an ideal qubit and in Fig. 3(b) for qubits with a finite dephasing time T_2. For small infidelities the results can be summarized as

$$\mathcal{F} \approx 1 - \frac{2}{3}\frac{\kappa_0}{\kappa} - \mathcal{C}_1\frac{\Gamma_{\text{th}}}{\kappa} - \mathcal{C}_2\frac{\kappa^2}{\omega_r^2} - \mathcal{C}_3\frac{\kappa}{\lambda^2 T_2}, \quad (7)$$

where individual errors arise from intrinsic cavity losses, mechanical noise, Stokes scattering, and the qubit dephasing, respectively. The numerical coefficients $\mathcal{C}_i \sim \mathcal{O}(1)$ (see Fig. 3) depend on the specific control pulse and can be optimized for a given set of experimental parameters.

Example.—We consider a microtoroidal cavity with a diameter $d = 20$ μm coupled to a doubly clamped SiN beam of dimensions $(l, w, t) \approx (15, 0.05, 0.05)$ μm. Optical quality factors of $Q_c \geq 2 \times 10^9$ [2,19] correspond to $\kappa_0/2\pi \leq 50$ kHz and $\kappa_f/2\pi \simeq 1$–5 MHz can be adjusted by the cavity-fiber separation. Depending on the tensile stress the first excited mechanical mode has a frequency of $\omega_r/2\pi \approx 5$–50 MHz and a zero point motion $a_0 \approx (1.6 - 0.6) \times 10^{-13}$ m, respectively. At $T = 100$ mK a mechanical quality factor of $Q_m \sim 2 \times 10^5$ corresponds to $\Gamma_{\text{th}}/2\pi \sim 10$ kHz and for these parameters the conditions Γ_{th}, $\kappa_0 \ll \kappa \ll \omega_r$ for a high quality OMT are

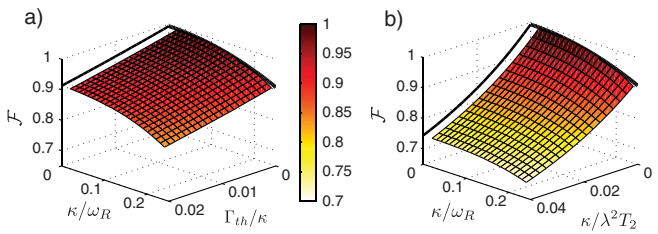

FIG. 3 (color online). (a) State transfer fidelity obtained from a numerical simulation of Eq. (4) for the control pulses shown in Fig. 2 and $\kappa_0 = 0$. (b) The same plot for $\Gamma_{\text{th}} = 0$ but including an exponential loss of qubit coherence $\sim e^{-t/T_2}$ during the transfer. From these two plots we extract the numerical coefficients $\mathcal{C}_1 \approx 4$, $\mathcal{C}_2 \approx 1.4$, and $\mathcal{C}_3 \approx 7.5$, which appear in the approximate expression of $\mathcal{F}$ given in Eq. (7).

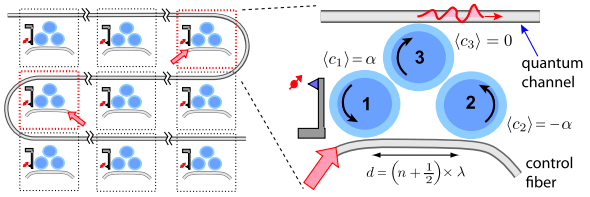

FIG. 4 (color online). Scalable quantum networks based on multimode OM transducers. At each node the three cavities are modeled by $H_c = \sum_{n=1}^{3} \Delta_n c_n^\dagger c_n + J(c_s^\dagger c_3 + \text{H.c.})$ where J is the tunneling coupling of mode c_3 with $c_s = (c_1 + c_2)/\sqrt{2}$. The driving field applied through the "control fiber" excites the asymmetric mode $c_a = (c_1 - c_2)/\sqrt{2}$ such that for $\Delta_1 = \Delta_2$ we obtain $\langle c_1\rangle = -\langle c_2\rangle = \alpha$ and $\langle c_3\rangle = 0$. The motion of the resonator modulates Δ_1 and induces a linearized OM coupling as given in Eq. (1) with the empty mode $c = (c_s + c_3)/\sqrt{2}$. Thereby, laser noise from the control fields does not affect the quantum channel and nodes can be selectively activated. The direction of the driving field is used to send photons into different directions to connect any two nodes of a large network.

satisfied. For electronic spin qubits dephasing times approaching $T_2 \approx 10$ ms have been demonstrated [20] and following Ref. [9] we estimate a magnetic coupling strength of $\lambda/2\pi \approx 50$ kHz. For superconducting charge qubits the electrostatic coupling can be substantially stronger, $\lambda/2\pi \approx 5$ MHz [12], while in current experiments $T_2 = 2$ μs [21]. The effective qubit splitting $\omega_q \sim \omega_r$ required for the control pulse described in Fig. 2 can be engineered using microwave-assisted qubit-resonator coupling schemes [9,11]. By choosing $(\kappa, \omega_r) = 2\pi \times (1, 5)$ MHz for the spin and $(\kappa, \omega_r) = 2\pi \times (5, 50)$ MHz for the charge qubit we obtain in both cases $\mathcal{F} \approx 0.85$. This shows that state transfer fidelities $\mathcal{F} > 2/3$ required for quantum communication [22] can be achieved with present technology. Near unit fidelities $\mathcal{F} \simeq 0.95$–0.99 can be expected from further optimizations of the system design and control pulses, or from communication protocols which, e.g., correct for photon loss errors [23].

In conclusion, we have described a universal approach for coherent light-matter interfaces based on OM transducers. In Fig. 4 we outline the concept of a multimode OM transducer using interference to separate the control fields from the quantum channel. This enables selective activation of individual nodes to realize large scale solid state or hybrid quantum networks. Beyond quantum communication, various other applications for OMTs can be considered such as new approaches to engineer single photon nonlinearites as well as optical readout and quantum measurement applications for optically nonactive quantum systems.

We gratefully acknowledge discussions with Klemens Hammerer. This work is supported by ITAMP, NSF, CUA, DARPA, the Packard Foundation, and the Danish National Research Foundation. K. S. and P. Z. acknowledge support by the Austrian Science Fund (FWF) through SFB FOQUS.

[1] J. I. Cirac *et al.*, Phys. Rev. Lett. **78**, 3221 (1997).
[2] H. J. Kimble, Nature (London) **453**, 1023 (2008).
[3] W. A. Coish and J. Baugh, Phys. Status Solidi B **246**, 2203 (2009).
[4] Y. Makhlin, G. Schön, and A. Shnirman, Rev. Mod. Phys. **73**, 357 (2001).
[5] D. Englund *et al.*, Nature (London) **450**, 857 (2007); K. Srinivasan and O. Painter, Nature (London) **450**, 862 (2007).
[6] G. Anetsberger *et al.*, Nature Phys. **5**, 909 (2009).
[7] M. Eichenfield *et al.*, Nature (London) **462**, 78 (2009).
[8] T. J. Kippenberg and K. J. Vahala, Science **321**, 1172 (2008).
[9] P. Rabl *et al.*, Phys. Rev. B **79**, 041302 (2009).
[10] H. J. Mamin *et al.*, Nature Nanotech. **2**, 301 (2007).
[11] A. D. Armour, M. P. Blencowe, and K. C. Schwab, Phys. Rev. Lett. **88**, 148301 (2002); E. K. Irish and K. Schwab, Phys. Rev. B **68**, 155311 (2003); I. Martin *et al.*, Phys. Rev. B **69**, 125339 (2004).
[12] M. D. LaHaye *et al.*, Nature (London) **459**, 960 (2009).
[13] C. W. Gardiner, Phys. Rev. Lett. **70**, 2269 (1993); H. J. Carmichael, Phys. Rev. Lett. **70**, 2273 (1993).
[14] J. M. Dobrindt, I. Wilson-Rae, and T. J. Kippenberg, Phys. Rev. Lett. **101**, 263602 (2008); S. Gröblacher *et al.*, Nature (London) **460**, 724 (2009); I. Wilson-Rae *et al.*, New J. Phys. **10**, 095007 (2008).
[15] K. Stannigel *et al.* (to be published)
[16] D. K. Armani *et al.*, Appl. Phys. Lett. **85**, 5439 (2004).
[17] I. Wilson-Rae *et al.*, Phys. Rev. Lett. **99**, 093901 (2007); F. Marquardt *et al.*, Phys. Rev. Lett. **99**, 093902 (2007).
[18] S. Gröblacher *et al.*, Nature Phys. **5**, 485 (2009); D. J. Wilson *et al.*, Phys. Rev. Lett. **103**, 207204 (2009); O. Arcizet *et al.*, Nature (London) **444**, 71 (2006); T. Rocheleau *et al.*, Nature (London) **463**, 72 (2010).
[19] S. M. Spillane *et al.*, Phys. Rev. A **71**, 013817 (2005); T. J. Kippenberg *et al.*, Appl. Phys. Lett. **85**, 6113 (2004).
[20] A. M. Tyryshkin *et al.*, Phys. Rev. B **68**, 193207 (2003); G. Balasubramanian *et al.*, Nature Mater. **8**, 383 (2009).
[21] J. A. Schreier *et al.*, Phys. Rev. B **77**, 180502(R) (2008); A. A. Houck *et al.*, Quant. Info. Proc. **8**, 105 (2009); F. Mallet *et al.*, Nature Phys. **5**, 791 (2009).
[22] S. Massar and S. Popescu, Phys. Rev. Lett. **74**, 1259 (1995).
[23] S. J. van Enk, J. I. Cirac, and P. Zoller, Phys. Rev. Lett. **78**, 4293 (1997); A. Sørensen and K. Mølmer, Phys. Rev. A **58**, 2745 (1998).